Cellular & Molecular Immunology www.nature.com/cmi

ARTICLE

# RRx-001 ameliorates inflammatory diseases by acting as a potent covalent NLRP3 inhibitor

Yun Chen[1], Hongbin He[1,2], Bolong Lin[1], Yun Chen[4], Xianming Deng[4], Wei Jiang[1] and Rongbin Zhou[1,3]

The NLRP3 inflammasome plays a crucial role in innate immune-mediated inflammation and contributes to the pathogenesis of multiple autoinflammatory, metabolic and neurodegenerative diseases, but medications targeting the NLRP3 inflammasome are not available for clinical use. RRx-001 is a well-tolerated anticancer agent currently being investigated in phase III clinical trials, but its effects on inflammatory diseases are not known. Here, we show that RRx-001 is a highly selective and potent NLRP3 inhibitor that has strong beneficial effects on NLRP3-driven inflammatory diseases. RRx-001 inhibits the activation of the canonical, noncanonical, and alternative NLRP3 inflammasomes but not the AIM2, NLRC4 or Pyrin inflammasomes. Mechanistically, RRx-001 covalently binds to cysteine 409 of NLRP3 via its bromoacetyl group and therefore blocks the NLRP3-NEK7 interaction, which is critical for the assembly and activation of the NLRP3 inflammasome. More importantly, RRx-001 treatment attenuates the symptoms of lipopolysaccharide (LPS)-induced systemic inflammation, dextran sulfate sodium (DSS)-induced colitis and experimental autoimmune encephalomyelitis (EAE) in mice. Thus, our study identifies RRx-001 as a new potential therapeutic agent for NLRP3-driven diseases.

**Keywords:** RRx-001; NLRP3 inflammasome; inflammatory diseases

*Cellular & Molecular Immunology* (2021) 18:1425–1436; https://doi.org/10.1038/s41423-021-00683-y

## INTRODUCTION

The NLR family pyrin domain containing 3 (NLRP3) inflammasome is an intracellular protein complex composed of the NOD-like receptor (NLR) family protein NLRP3, adapter protein ASC and cysteine protease caspase-1.[1,2] As an innate immune sensor, NLRP3 responds to a wide range of stimuli derived from pathogens, the environment and the host.[3] Upon activation, NLRP3 recruits ASC and pro-caspase-1 to assemble the NLRP3 inflammasome, which results in autoproteolysis of caspase-1. Active caspase-1 mediates proteolytic cleavage of pro-IL-1β and pro-IL-18 to their mature forms and drives pyroptosis, a form of inflammatory cell death.[4] It has been reported that aberrant activation of the NLRP3 inflammasome leads to a variety of human inflammatory disorders, such as gout, chronic liver disease, type 2 diabetes (T2D), neurodegenerative diseases, atherosclerosis and inflammatory bowel disease (IBD).[5–14] NLRP3 is therefore a potential therapeutic target for these diseases.

To develop strategies for treating NLRP3-driven diseases, researchers have identified several NLRP3-targeted inhibitors with potentially beneficial effects, including 3,4-methylenedioxy-β-nitrostyrene (MNS), MCC950, CY-09, tranilast, oridonin and OLT1177.[15–21] However, most of these inhibitors are not available for clinical use. MNS, CY-09 and oridonin have not reached the clinical trial stage. The MCC950-related compounds, namely, IZD334 (ClinicalTrials.gov Identifier: NCT04086602) and inzomelid (NCT04015076), have recently completed phase I clinical trials. IFM-2427, acquired by Novartis, is in a phase I clinical trial.[22] Tranilast (NCT03923140) has entered a phase II clinical trial to treat cryopyrin-associated periodic syndrome (CAPS). OLT1177, an active β-sulfonyl nitrile, is being studied in a phase II clinical trial to treat acute gouty arthritis.[23] Although research on targeting the NLRP3 inflammasome is developing rapidly, whether these agents can be used to treat NLRP3-related diseases in humans remains to be determined. Therefore, there is still a need for NLRP3 inhibitors that are closer to clinical application and have a favorable safety profile.

RRx-001 (1-bromoacetyl-3,3-dinitroazetidine) is an anticancer agent currently in phase III clinical trials and was developed by the aerospace industry.[24] Clinical studies have shown that RRx-001 can be used to treat a variety of tumors, such as those of brain cancer, colorectal cancer, small-cell lung cancer and non-small cell lung cancer.[25–29] In addition to its cytotoxic antiproliferative effects on tumor cells, RRx-001 exerts anticancer effects by acting as a radiosensitizer, chemosensitizer, or immunosensitizer.[25–27,30] Mechanistically, RRx-001 effectively catalyzes the production of nitric oxide (NO) and reactive oxygen species (ROS), alters the intracellular redox status, and promotes epigenetic modulation.[31–33] Through these mechanisms, RRx-001 reprograms the tumor microenvironment by

[1]Hefei National Laboratory for Physical Sciences at Microscale, the CAS Key Laboratory of Innate Immunity and Chronic Disease, School of Basic Medical Sciences, Division of Life Sciences and Medicine, University of Science and Technology of China, Hefei, China; [2]Department of Geriatrics, Gerontology Institute of Anhui Province, the First Affiliated Hospital of USTC, Division of Life Sciences and Medicine, University of Science and Technology of China, Hefei, China; [3]CAS Centre for Excellence in Cell and Molecular Biology, University of Science and Technology of China, Hefei, China and [4]State Key Laboratory of Cellular Stress Biology, Innovation Center for Cell Signaling Network, School of Life Sciences, Xiamen University, Xiamen, Fujian, China
Correspondence: Wei Jiang (ustcjw@ustc.edu.cn) or Rongbin Zhou (zrb1980@ustc.edu.cn)
These authors contributed equally: Yun Chen, Hongbin He

Received: 4 December 2020 Accepted: 11 April 2021
Published online: 10 May 2021

regulating angiogenesis, vascular normalization[34] and tumor-associated macrophage (TAM) polarization.[35] RRx-001 has also been shown to protect normal tissues but not tumor tissues by upregulating the expression of the antioxidant gene Nrf2 in normal tissues.[36] More importantly, RRx-001 elicited no systemic toxicity during the treatment of over 300 patients with multiple tumors,[28,37] suggesting that RRx-001 is a well-tolerated agent without clinically significant toxic effects. Although RRx-001 has shown promising anticancer activities, its effects and targets in inflammatory diseases have not been reported.

In this study, we showed that RRx-001 is a highly potent NLRP3 inhibitor. RRx-001 covalently binds to cysteine 409 of NLRP3 to inhibit NLRP3 inflammasome assembly by blocking the interaction between NLRP3 and NEK7. RRx-001 was efficacious in mouse models of NLRP3-associated pathologies and diseases, such as LPS-induced systemic inflammation, DSS-induced colitis and EAE. These findings suggest that RRx-001 is a potential therapeutic agent for NLRP3-related diseases.

## RESULTS

### RRx-001 is a highly potent inhibitor of the NLRP3 inflammasome

To determine the effects of RRx-001 on NLRP3 inflammasome activation, we pretreated LPS-primed bone marrow-derived macrophages (BMDMs) with RRx-001 for 30 min and then stimulated the cells with the NLRP3 agonist nigericin (3 μM). We found that RRx-001 dose-dependently blocked IL-1β secretion, caspase-1 cleavage and cell death at concentrations of 100–300 nM (Fig. 1A–C). However, induction of TNF-α and IL-6 expression by LPS was not impaired by RRx-001 (Fig. 1D, E), suggesting that its inhibitory effect on IL-1β is specific under this condition. As NLRP3 inflammasome activation can be triggered by a wide range of stimuli, we then investigated the effects of RRx-001 on NLRP3 inflammasome activation triggered by other agonists. Our results showed that RRx-001 suppressed IL-1β secretion and caspase-1 cleavage induced by monosodium urate crystals (MSU) and ATP (Fig. 1F, G). RRx-001 also inhibited potassium efflux-independent NLRP3 inflammasome activation caused by CL097[38] (Supplementary Fig. 1A). In addition, noncanonical NLRP3 inflammasome activation triggered by cytosolic LPS (cLPS) was suppressed by RRx-001 (Supplementary Fig. 1B, C). These results suggest that RRx-001 exerts a broad-spectrum inhibitory effect on NLRP3 inflammasome activation. However, RRx-001 did not inhibit NLRP3-independent cell death induced by cLPS (Supplementary Fig. 1D). We also treated human peripheral blood mononuclear cells (PBMCs) with RRx-001 and then induced NLRP3 activation with nigericin or LPS alone. We found that RRx-001 suppressed the secretion of IL-1β (Fig. 1H and Supplementary Fig. 1E) but not TNF-α (Fig. 1I and Supplementary Fig. 1F) in PBMCs. Taken together, these findings confirmed that RRx-001 blocks NLRP3 inflammasome activation in both murine and human cells.

To determine whether RRx-001 can inhibit other inflammasomes, LPS-primed BMDMs were pretreated with RRx-001 and were then transfected with poly(A/T) to activate the AIM2 inflammasome or infected with *Salmonella typhimurium* to activate the NLRC4 inflammasome. Our data showed that RRx-001 had no effect on AIM2 and NLRC4 inflammasome activation (sup Fig. 1G, H). We also found that RRx-001 could not suppress Pyrin inflammasome activation induced by *Clostridium difficile* toxin B (TcdB) (Supplementary Fig. 1I). Collectively, these results suggested that RRx-001 specifically inhibits NLRP3 inflammasome activation.

It has been reported that RRx-001 suppresses pro-IL-1β expression by altering the metabolic process in macrophages,[39] and thus, we tested whether RRx-001 blocks NLRP3 inflammasome activation by suppressing NF-κB-dependent pro-IL-1β and NLRP3 expression. Treating BMDMs with RRx-001 at concentrations of 100–300 nM before or after LPS stimulation had no effect on the expression of pro-IL-1β or NLRP3 (Supplementary Fig. 2A) and did not affect the production of IL-6 or TNF-α (Supplementary Fig. 2B, C), suggesting that the concentrations at which RRx-001 inhibits the NLRP3 inflammasome are not sufficient to inhibit the LPS-induced priming process. We also observed that treatment with higher concentrations (0.5–2 μM) of RRx-001 before LPS stimulation indeed decreased pro-IL-1β expression and IL-6 production but did not attenuate NLRP3 expression or TNF-α production (Supplementary Fig. 3A–C). The inhibitory effect of RRx-001 on IL-6 release was ~8 times less potent than that on IL-1β release (Supplementary Fig. 3D, E). In addition, treatment with higher concentrations (0.5–2 μM) of RRx-001 after 3 h of LPS stimulation had no effect on the expression of pro-IL-1β and NLRP3 or the production of IL-6 and TNF-α (Supplementary Fig. 3A–C).

### RRx-001 inhibits NLRP3 inflammasome assembly by blocking the NLRP3-NEK7 interaction

We next studied the underlying mechanism of RRx-001's effects on the NLRP3 inflammasome. It has been proposed that RRx-001 can reduce the activity of G6PD to disrupt the pentose phosphate pathway in tumor cells.[40] We found that NLRP3 inflammasome activation and the inhibitory activity of RRx-001 were not abrogated when *G6pdx* was silenced by siRNA (Supplementary Fig. 4A–C). Moreover, the G6PD inhibitor dehydroepiandrosterone (DHEA) had no effect on NLRP3 inflammasome activation (Supplementary Fig. 4D). These results indicated that inhibition of G6PD is not essential for inhibition of the NLRP3 inflammasome by RRx-001.

Potassium efflux and chloride efflux have been reported as upstream signaling events of NLRP3 inflammasome activation.[41–44] To investigate whether RRx-001 can impact these events, we examined intracellular potassium and chloride efflux after nigericin (3 μM) stimulation. Our data revealed that nigericin-induced efflux of potassium and chloride was not prevented by RRx-001 (Supplementary Fig. 5A, B). In addition, nigericin-stimulated BMDMs were stained to detect mitochondrial damage, which is another upstream signaling event of NLRP3 inflammasome activation.[45,46] No significant decreases in mitochondrial damage or ROS production were observed after RRx-001 pretreatment (Supplementary Fig. 5C). These results suggest that RRx-001 acts downstream of the upstream events mentioned above to block NLRP3 activation.

We then considered the possibility that RRx-001 blocks the assembly of the NLRP3 inflammasome. We first examined the formation of ASC oligomers, an important step for subsequent caspase-1 cleavage.[47,48] Similar to the results obtained previously (Fig. 1B), RRx-001 blocked IL-1β secretion and caspase-1 cleavage (Fig. 2A). Consistent with this finding, RRx-001 attenuated ASC oligomerization in a concentration-dependent manner (Fig. 2A), suggesting that RRx-001 exerts an inhibitory effect on NLRP3 activation upstream of ASC oligomerization. The interaction between NLRP3 and ASC is essential for the recruitment of ASC to NLRP3.[1,2] Immunoprecipitation assays were used to test the nigericin-induced NLRP3-ASC interaction and showed that RRx-001 substantially inhibited the endogenous NLRP3-ASC interaction (Fig. 2B).The NLRP3-NEK7 interaction is another critical step occurring upstream of NLRP3 oligomerization and ASC recruitment.[49–51] We found that RRx-001 also suppressed the endogenous interaction between NLRP3 and NEK7 (Fig. 2C). These results indicated that RRx-001 might inhibit the assembly of the NLRP3 inflammasome by blocking the interaction between NLRP3 and NEK7. We employed an overexpression system in HEK-293T cells to test this hypothesis. The results showed that RRx-001 prevented the direct interaction between NLRP3 and NEK7 (Fig. 2D) but not the NLRP3-NLRP3 interaction (Fig. 2E) or the NLRP3-ASC interaction (Fig. 2F), indicating that RRx-001 directly inhibits the NLRP3-NEK7 interaction but does not inhibit NLRP3 oligomerization or ASC recruitment. Consistent with this finding, RRx-001 did not

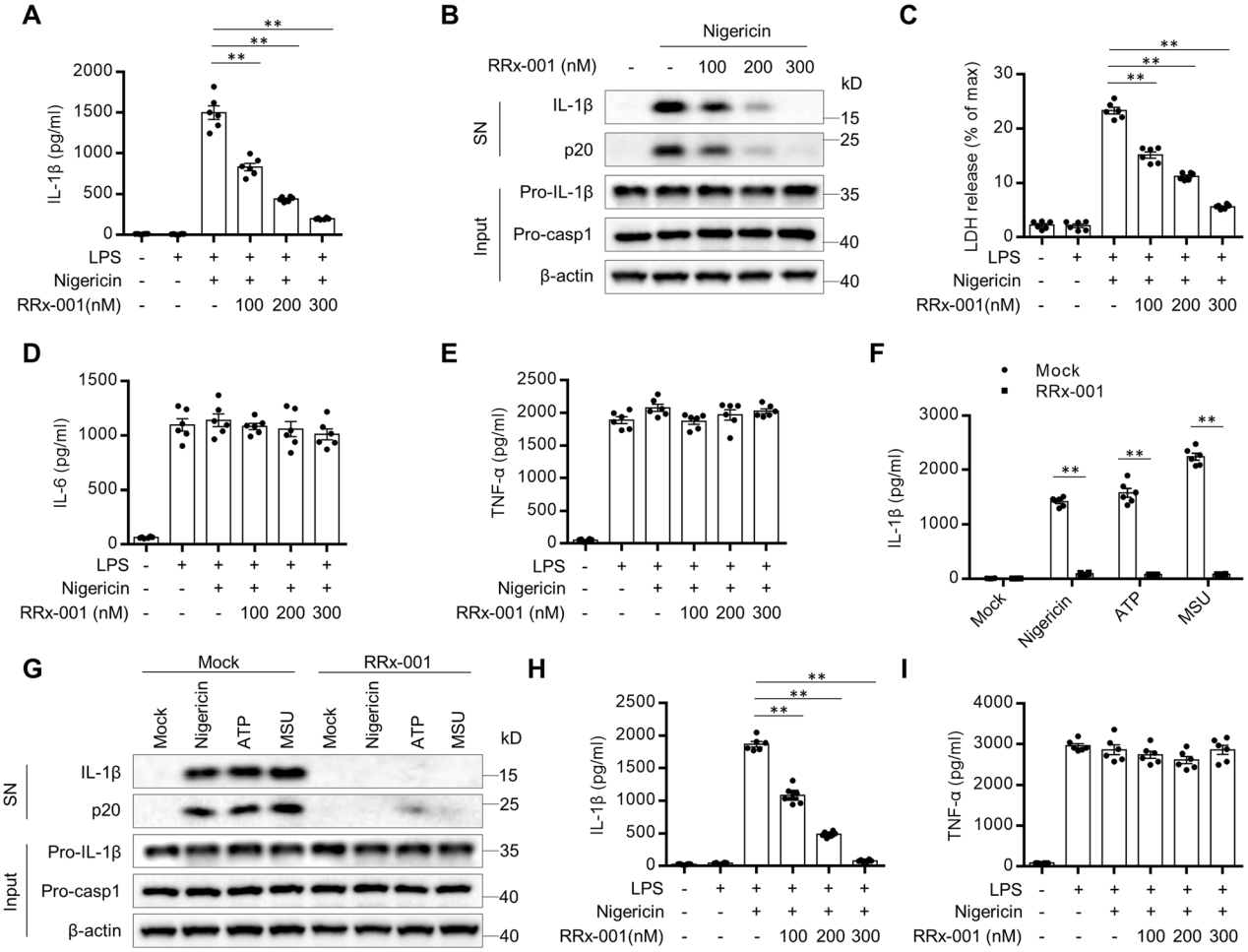


**Fig. 1 RRx-001 inhibits NLRP3 inflammasome activation. A–E** LPS-primed BMDMs were pretreated with RRx-001 at different concentrations for 30 min and were then stimulated with nigericin (3 μM). **A** ELISA of mature IL-1β in the supernatants of BMDMs. **B** Western blot analysis of mature IL-1β and cleaved caspase-1 (p20) in supernatants (SN) of BMDMs and of pro-IL-1β and pro-caspase-1 in the lysates (Input) of BMDMs. **C** LDH release in the supernatants of BMDMs. ELISA of IL-6 (**D**) and TNF-α (**E**) in the SN of BMDMs. **F**, **G** LPS-primed BMDMs were pretreated with or without RRx-001 (300 nM) for 30 min and were then stimulated with nigericin, ATP or MSU. **F** ELISA of mature IL-1β in the SN of BMDMs. **G** Western blot analysis of mature IL-1β and cleaved caspase-1 in the SN of BMDMs and of pro-IL-1β and pro-caspase-1 in the lysates (Input) of BMDMs. **H**, **I** LPS-primed PBMCs were pretreated with RRx-001 at different concentrations for 30 min and were then stimulated with nigericin (3 μM). ELISA of IL-1β (**H**) and TNF-α (**I**) in the SN of PBMCs. The data are from three independent experiments with biological duplicates in each and are shown as the mean ± SEM values ($n = 3$) (**A**, **C**–**F**, **H**, **I**) or are representative of three independent experiments (**B**, **G**). Statistical significance was analyzed by the Mann–Whitney test: $^{**}P < 0.01$

affect the ATPase activity of NLRP3 (Supplementary Fig. 6A). NEK7 has been proposed to contribute to mitotic spindle assembly by interacting with NEK9,[52] but we found that RRx-001 did not impact the NEK7-NEK9 interaction in HEK-293T cells (Supplementary Fig. 6B). These results demonstrated that RRx-001 inhibits NLRP3 inflammasome assembly by directly blocking the NLRP3-NEK7 interaction.

RRx-001 activity depends on both the twin $NO_2$ and bromoacetyl groups

We next sought to determine which functional group in RRx-001 could be responsible for the inhibitory effect of RRx-001 on NLRP3 activation. We first removed the twin $NO_2$ groups in RRx-001 and named the new compound C-0 (Fig. 3A). C-0 retained the potential to inhibit NLRP3 inflammasome activation, but the concentration required was higher than that of RRx-001 (Fig. 3B, C). The inhibitory activity of C-0 was approximately 32 times lower than the activity of RRx-001 (Supplementary Fig. 7A). These results indicated that the twin $NO_2$ groups in RRx-001 improved the inhibitory activity but did not determine the inhibitory capacity of RRx-001.

We then investigated whether the bromoacetyl group in RRx-001 determines the inhibitory effect of RRx-001. Additional chemical modifications of the bromoacetyl group of C-0 were performed: we added a methyl group to the bromoacetyl group (C-1), replaced the bromine atom with a chlorine atom (C-2) or removed the bromine atom (C-3) (Fig. 3D). These alterations abolished the potency of C-0 to inhibit NLRP3 inflammasome activation (Fig. 3E, F), indicating that the bromoacetyl group is essential for RRx-001-mediated inhibition of the NLRP3 inflammasome.

Since the bromoacetyl group determines the inhibitory effect of RRx-001, we next investigated the reversibility of the inhibitory effect of RRx-001. After treating LPS-primed BMDMs with RRx-001 for 15 min, we washed the cells three times every five minutes to remove unbound agent and then stimulated the cells with nigericin (3 μM). We found that RRx-001 inhibited the NLRP3 inflammasome independent of washing (Fig. 3G). The same results were observed in the washout assay of C-0 (Fig. 3H), indicating that the inhibitory effect of RRx-001 determined by the bromoacetyl group is irreversible. Thus, our results suggest that

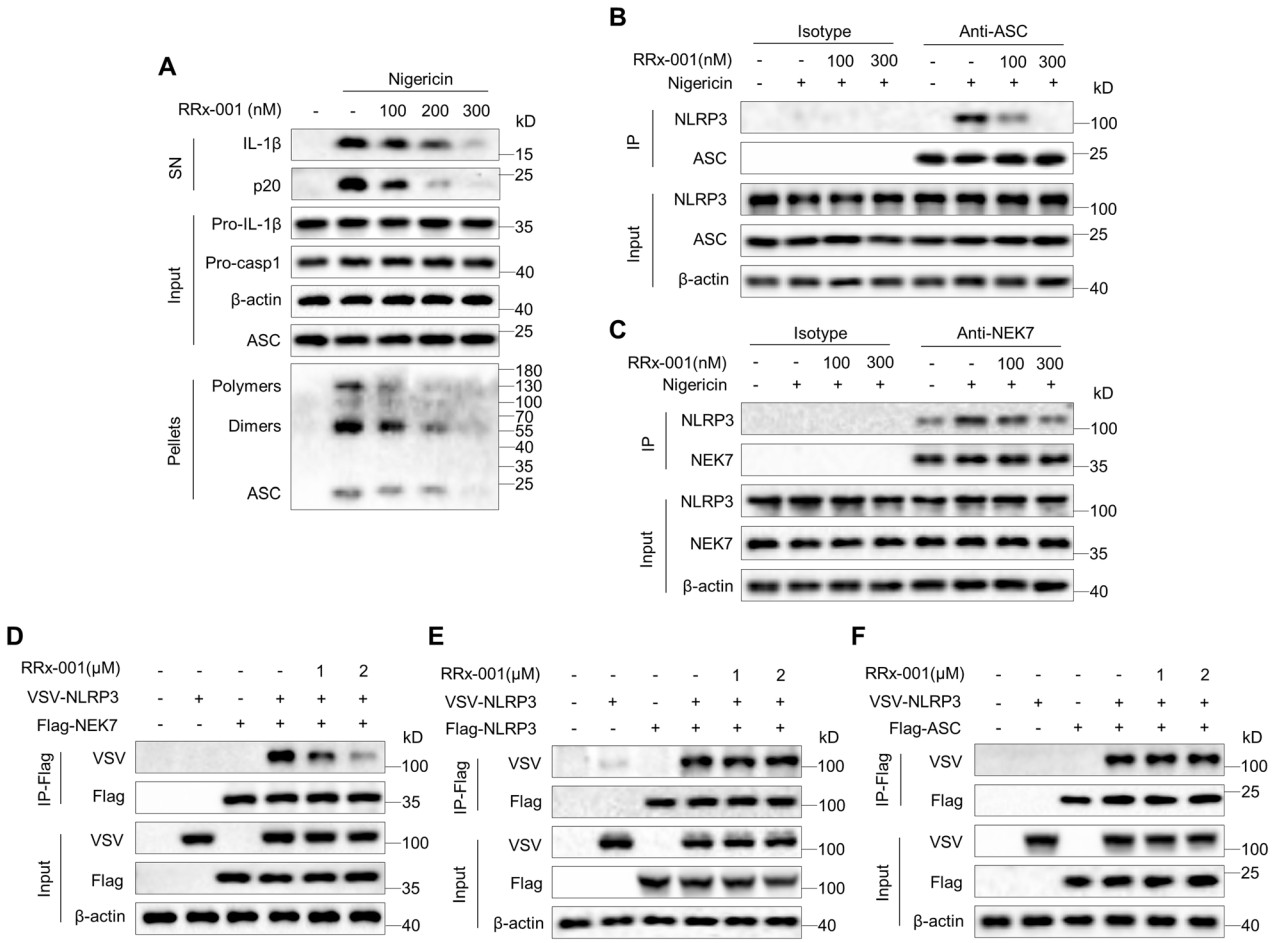


**Fig. 2 RRx-001 suppresses NLRP3 inflammasome assembly by blocking the NEK7–NLRP3 interaction. A** Western blot analysis of crosslinked ASCs in the NP-40–insoluble pellet of LPS-primed BMDMs pretreated with RRx-001 at different concentrations and then stimulated with nigericin (3 μM). **B** Endogenous immunoprecipitation (IP) and western blot analysis to evaluate the NLRP3-ASC interaction in LPS-primed BMDMs pretreated with RRx-001 at different concentrations and then stimulated with nigericin (3 μM). **C** Endogenous immunoprecipitation (IP) and western blot analysis to evaluate the NLRP3-NEK7 interaction in LPS-primed BMDMs pretreated with RRx-001 at different concentrations and then stimulated with nigericin (3 μM). **D** IP and western blot analysis to evaluate the NEK7–NLRP3 interaction in the lysates of HEK-293T cells treated with RRx-001 at different concentrations. **E** IP and western blot analysis to evaluate the NLRP3-NLRP3 interaction in the lysates of HEK-293T cells treated with RRx-001 at different concentrations. **F** IP and western blot analysis to evaluate the ASC-NLRP3 interaction in the lysates of HEK-293T cells treated with RRx-001 at different concentrations. All data are representative of three independent experiments

RRx-001 might covalently bind to its target protein via its bromoacetyl group.

### RRx-001 covalently binds to cysteine 409 in the NLRP3 NACHT domain

Next, we sought to identify the target protein of RRx-001. Since RRx-001 blocks the interaction between NLRP3 and NEK7, we hypothesized that RRx-001 might directly target NLRP3 or NEK7. To confirm this hypothesis, we employed the drug affinity responsive target stability (DARTS) technique, which is based on the reduction in protease susceptibility of a target protein upon drug binding.[53] We observed that RRx-001 protected NLRP3 from protease-mediated proteolysis in a concentration-dependent manner (Fig. 4A), indicating that there is an interaction between RRx-001 and NLRP3. Other components of the NLRP3 inflammasome, including NEK7, ASC and pro-caspase-1, were not protected in the presence of RRx-001 (Fig. 4A), suggesting that RRx-001 selectively targets NLRP3. Consistent with the previous results indicating that the bromoacetyl group determines the inhibitory effect of RRx-001 (Fig. 3D–F), C-0 could interact with NLRP3, while other compounds lacking the bromoacetyl group could not (Fig. 4B), indicating that RRx-001 covalently binds to NLRP3 via its bromoacetyl group. We used a microscale thermophoresis (MST) assay to further confirm the direct interaction between RRx-001 and purified GFP-NLRP3. The data showed that the equilibrium dissociation constant ($K_D$) was ~20.8 nM (Fig. 4C), suggesting high-affinity binding between RRx-001 and purified GFP-NLRP3. We also performed DARTS using HEK-293T cells expressing NLRP3 or other inflammasome sensors and found that RRx-001 specifically interacted with NLRP3 but not AIM2, NLRC4 or NLRP1b (Fig. 4D–G).

Further DARTS experiments showed that RRx-001 binds to the NACHT domain but not the PYD or LRR domain of NLRP3 (Fig. 5A–C).

It has been proposed that RRx-001's bromoacetyl group is selectively reactive with the cysteine of glutathione and cysteine 93 of hemoglobin.[54] Thus, a cysteine within the NACHT domain might be the binding site of RRx-001. Using NACHT mutants in which a cysteine was substituted with an alanine, we sought to identify which cysteine residue in NLRP3 binds to RRx-001. The DARTS results showed that RRx-001 interacted with all NACHT mutants except the C409A NACHT mutant (Fig. 5D, Supplementary Fig. 8A). In addition, although the C409A mutation did not

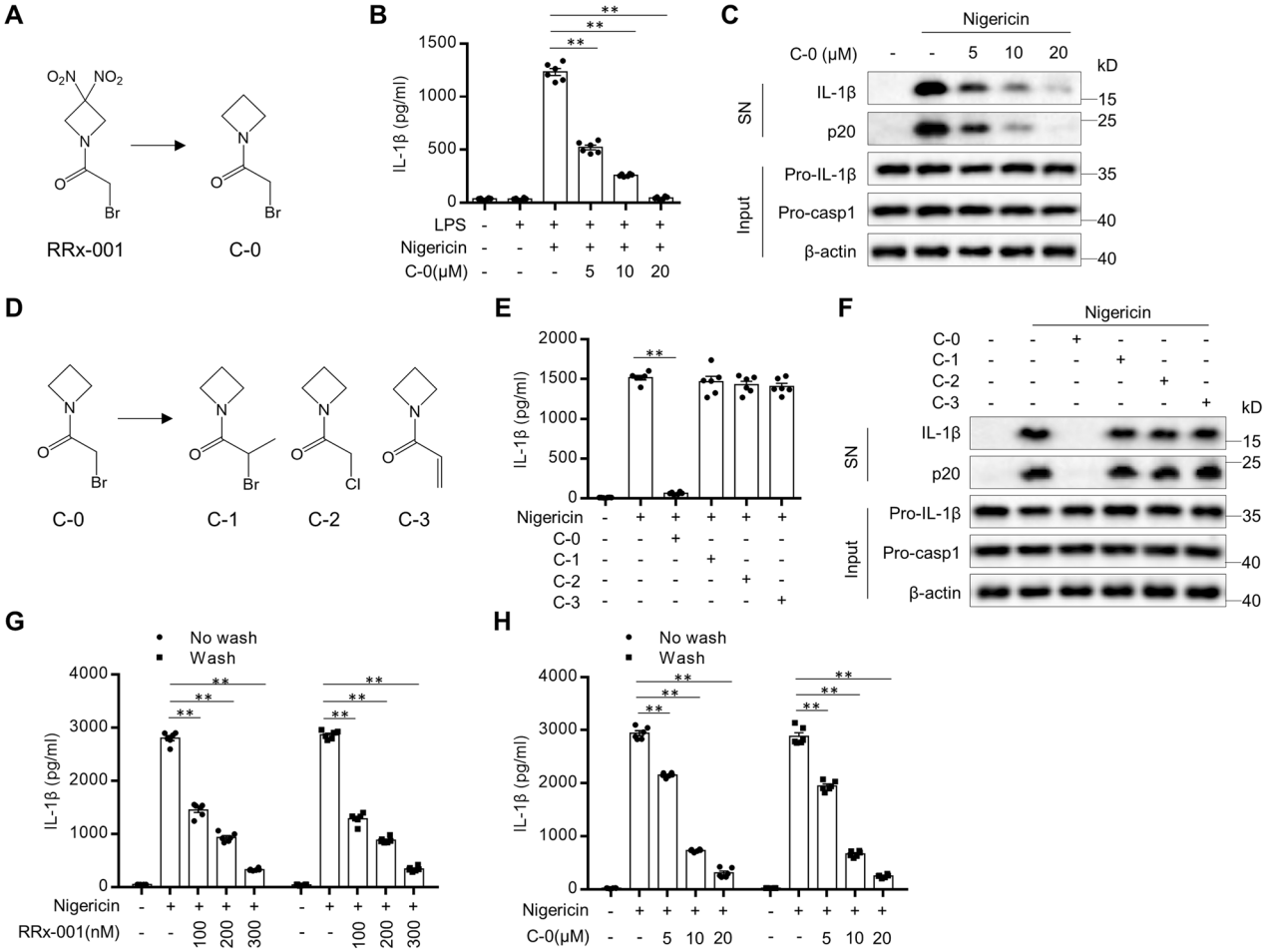


**Fig. 3 RRx-001's activity depends on both the twin $NO_2$ and bromoacetyl groups. A** Structure of RRx-001 without the twin $NO_2$ groups (C-0). **B, C** LPS-primed BMDMs were pretreated with C-0 at different concentrations for 30 min and were then stimulated with nigericin (3 μM). **B** ELISA of mature IL-1β in the SN of BMDMs. **C** Western blot analysis of mature IL-1β and cleaved caspase-1 in the SN of BMDMs and of pro-IL-1β and pro-caspase-1 in the lysates (Input) of BMDMs. **D** Structures of C-0 with modifications to the bromoacetyl group (C-1, C-2, C-3). **E, F** LPS-primed BMDMs were pretreated with 20 μM C-0, C-1, C-2 or C-3 for 30 min and were then stimulated with nigericin (3 μM). **E** ELISA of mature IL-1β in the SN of BMDMs. **F** Western blot analysis of mature IL-1β and cleaved caspase-1 in the SN of BMDMs and of pro-IL-1β and pro-caspase-1 in the lysates (Input) of BMDMs. ELISA of mature IL-1β in the SN of LPS-primed BMDMs pretreated with RRx-001 (**G**) or C-0 (**H**) at different concentrations for 15 min, washed three times, and then stimulated with nigericin (3 μM). The data are from three independent experiments with biological duplicates in each and are shown as the mean ± SEM values ($n = 3$) (**B**, **E**, **G**, **H**) or are representative of three independent experiments (**C**, **F**). Statistical significance was analyzed by the Mann–Whitney test: $^{**}P < 0.01$

affect the NLRP3-NEK7 interaction, this interaction was not blocked by RRx-001 (Fig. 5E). We also found that RRx-001 inhibited activation of the NLRP3 inflammasome in NLRP3-deficient macrophages reconstituted with WT NLRP3 but not in NLRP3-deficient macrophages reconstituted with mutant NLRP3 (C405A) (Fig. 5F, G). Collectively, these results indicate that RRx-001's bromoacetyl group covalently binds to cysteine 409 of human NLRP3 and cysteine 405 of mouse NLRP3.

## RRx-001 suppresses LPS-induced systemic inflammation, DSS-induced colitis and EAE

To examine the therapeutic potential of RRx-001 in vivo, we then tested the effect of RRx-001 in NLRP3-mediated disease models. Mice were treated with or without RRx-001 before challenge with LPS to induce septic shock, which is a well-characterized model of NLRP3-driven inflammation.[55] The data showed that RRx-001 treatment significantly reduced the IL-1β level in serum (Supplementary Fig. 9A) but had only a mild effect on the serum TNF-α level, which was inflammasome-independent (Supplementary Fig. 9B). These results suggest that RRx-001 can inhibit LPS-induced NLRP3 inflammasome activation in vivo.

The NLRP3 inflammasome has been considered an important contributor to dextran sulfate sodium (DSS)-induced colitis,[12] a mouse model of human IBD. DSS-treated mice were intraperitoneally injected with RRx-001 or vehicle once a day, and the body weight and disease activity index (DAI) were monitored. RRx-001 treatment markedly ameliorated weight loss and DAI during DSS-induced colitis in a dose-dependent manner (Fig. 6A, B). In addition, colon shortening, which is the macroscopic pathological feature of colitis, was inhibited by RRx-001 (Fig. 6C). Histological analysis revealed that RRx-001 treatment decreased the destruction of the intestinal epithelium and infiltration of immune cells (Fig. 6D). The level of IL-1β in serum was also decreased in the presence of RRx-001, suggesting the inhibitory effect of RRx-001 on the NLRP3 inflammasome in vivo (Fig. 6E). Collectively, these results indicate that RRx-001 effectively alleviates DSS-induced colitis in mice.

Considering the important role of the NLRP3 inflammasome in the EAE mouse model,[56,57] which highly mimics human multiple sclerosis, we tested whether RRx-001 is effective in treating EAE. C57BL/6J mice were intraperitoneally injected with RRx-001 or vehicle along with EAE induction. RRx-001 treatment prevented

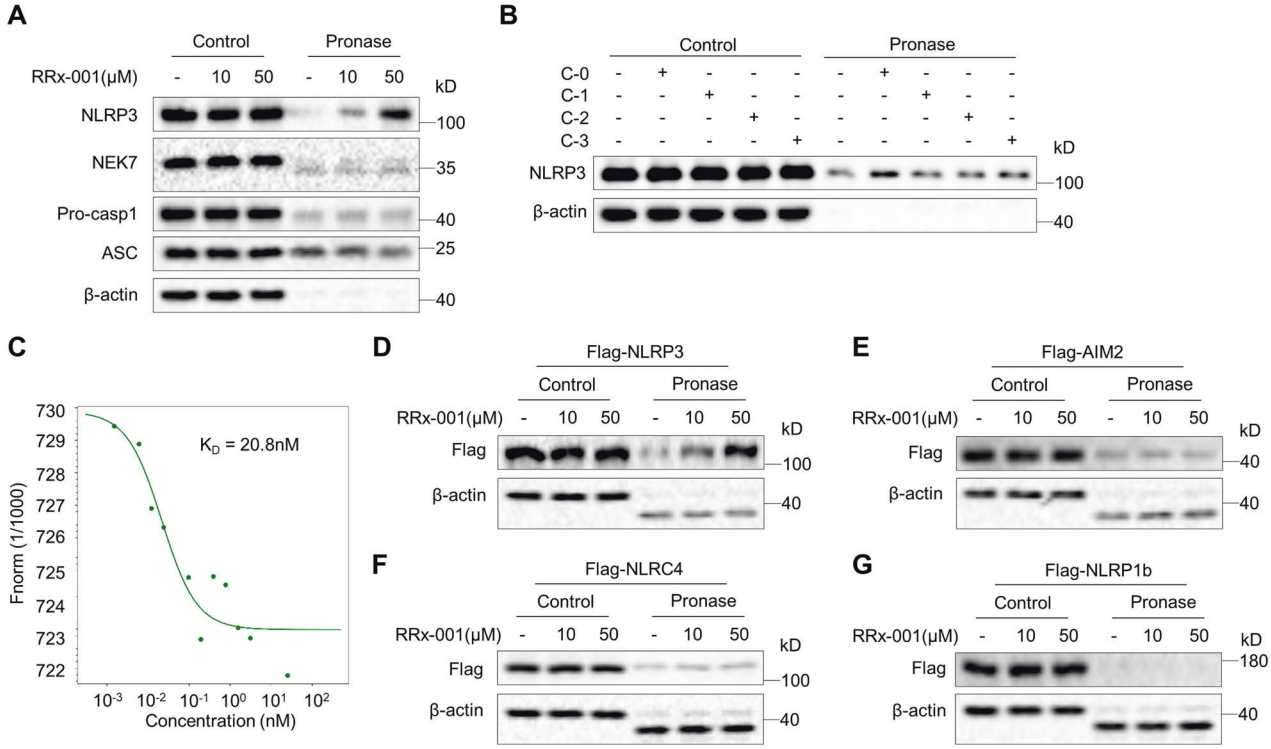


**Fig. 4 RRx-001 directly binds to NLRP3. A** LPS-primed BMDMs were lysed and incubated with RRx-001 at different concentrations. A DARTS assay was performed with pronase (25 ng/μg of protein), and NLRP3, NEK7, pro-caspase-1 and ASC in lysates were analyzed by western blotting. **B** LPS-primed BMDMs were lysed and incubated with 200 μM C-0, C-1, C-2 or C-3. A DARTS assay was performed with pronase (25 ng/μg of protein), and NLRP3 in lysates was analyzed by western blotting. **C** MST assay to evaluate the affinity between RRx-001 and purified GFP-NLRP3 protein. HEK-293T cells transfected with Flag-tagged NLRP3 (**D**), AIM2 (**E**), NLRC4 (**F**) or NLRP1b (**G**) were lysed and incubated with or without RRx-001 (50 μM). A DARTS assay was performed with pronase (25 ng/μg of protein), and lysates were analyzed by western blotting. All data are representative of three independent experiments

the clinical course of EAE and reduced inflammatory infiltration and demyelination in the spinal cord in treated mice compared with mice in the vehicle control group (Fig. 7A, B). Mice administered RRx-001 showed significantly reduced frequencies and numbers of infiltrating $CD4^+$, $CD8^+$, $CD11b^+$ and $CD11b^-$ cells gated on $CD45^{hi}$ cells in the CNS (Fig. 7C, D). In addition, the expression levels of proinflammatory cytokines, including IL-1β, IL-6 and TNF-α, in the CNS were reduced by RRx-001 treatment (Fig. 7E). Collectively, these data indicate that RRx-001 protects mice from the pathogenesis of EAE, as evidenced by the strong attenuation of disease severity and inflammation. To test whether this effect of RRx-001 is mediated by NLRP3 inhibition, we treated *Nlrp3*$^{-/-}$ mice with RRx-001 or vehicle along with EAE induction. The results showed that RRx-001 treatment did not affect the clinical course of EAE or the infiltration of immune cells in the CNS of *Nlrp3*$^{-/-}$ mice (Supplementary Fig. 10A, B), suggesting that RRx-001 ameliorates inflammatory diseases by acting as an NLRP3 inhibitor.

## DISCUSSION

In this study, we demonstrated that RRx-001, an anticancer agent currently in phase III trials, can strongly inhibit NLRP3 inflammasome activation and is effective in the treatment of NLRP3-driven diseases in mouse models. This finding may provide new therapeutic approaches for NLRP3-driven diseases and suggests that RRx-001 is a versatile agent that can be used in the treatment of inflammatory diseases in addition to cancer.

Our results indicated that RRx-001 directly binds to NLRP3 to inhibit the assembly of the NLRP3 inflammasome, suggesting that RRx-001 is a direct NLRP3 inhibitor. Although previous studies have proposed several small molecules that directly target NLRP3 and show some benefit in NLRP3-associated diseases,[15–21] no therapies are currently available for clinical use. Our study indicated that RRx-001 is an agent with increased efficacy and safety to treat these diseases. RRx-001 inhibited IL-1β production with an IC50 value of 116.9 nM, indicating that it is more potent than most other NLRP3 inhibitors. In addition, we found that intraperitoneal administration of RRx-001 at a dosage of 10 mg/kg/day (equivalent to a dosage of 0.9 mg/kg/day in humans) had significant therapeutic effects on DSS-induced colitis and EAE in mice. RRx-001 has shown promising effects in cancer treatment and has been proven to have low toxicity and safety in clinical trials.[37]

RRx-001 has been proposed to suppress the expression of pro-IL-1β by affecting the metabolic process of macrophages.[39] However, our data showed that the concentrations required for inhibition of the NLRP3 inflammasome were not sufficient to inhibit LPS-induced pro-IL-1β expression. The inhibitory activity of RRx-001 against IL-1β release was ~8 times more potent than that on IL-6 release induced by LPS. Thus, RRx-001 might be more effective in the treatment of NLRP3-dependent inflammatory diseases than in the treatment of other inflammatory diseases.

Our data showed that RRx-001 can inhibit NLRP3 inflammasome assembly by blocking the interaction between NLRP3 and NEK7. It is possible that RRx-001 might target the interface between NLRP3 and NEK7. However, our data showed that cysteine 409, which is not on the interface between NLRP3 and NEK7 according to a cryoelectron structure of human NLRP3 in complex with NEK7,[58] is the binding site of RRx-001. Thus, RRx-001 does not directly target the interface between NLRP3 and NEK7. One possible mechanism

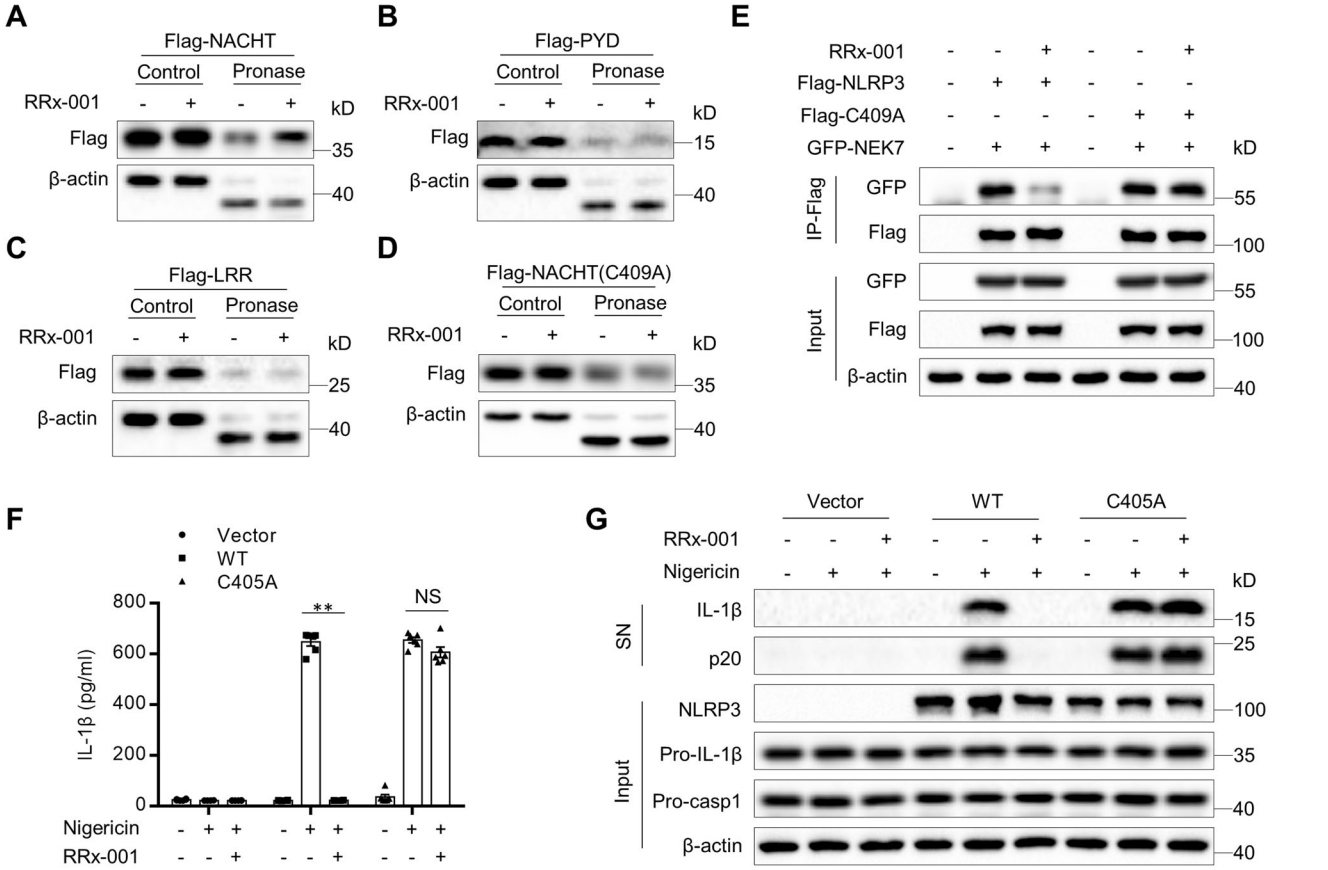


**Fig. 5 RRx-001 binds to cysteine 409 of NLRP3.** HEK-293T cells transfected with Flag-tagged NLRP3-NACHT (**A**), NLRP3-PYD (**B**), NLRP3-LRR (**C**) or NLRP3-NACHT (C409) (**D**) were lysed and incubated with or without RRx-001 (50 μM). A DARTS assay was performed with pronase (25 ng/μg of protein), and lysates were analyzed by western blotting. **E** IP and western blot analysis to evaluate the interaction between NEK7 and WT or mutant NLRP3 (C409A) in the lysates of HEK-293T cells treated with or without RRx-001 (2 μM). **F, G** LPS-primed *Nlrp3*$^{-/-}$ BMDMs reconstituted with WT or mutant NLRP3 (C409A) were pretreated with RRx-001 (300 nM) for 30 min and were then stimulated with nigericin (3 μM). **F** ELISA of mature IL-1β in the SN of BMDMs. **G** Western blot analysis of mature IL-1β and cleaved caspase-1 in the SN of BMDMs and of pro-IL-1β and pro-caspase-1 in the lysates (Input) of BMDMs. The data are from three independent experiments with biological duplicates in each and are shown as the mean ± SEM values ($n = 3$) (**F**) or are representative of three independent experiments (**A**–**E**, **G**). Statistical significance was analyzed by the Mann–Whitney test: $^{**}P < 0.01$; NS not significant

is that RRx-001 might trigger a conformational change in NLRP3 and thereby inhibit the interaction between NLRP3 and NEK7. However, the detailed mechanisms by which RRx-001 affects the NLRP3 conformation need to be further investigated.

Our results indicated that the twin $NO_2$ groups in RRx-001 improved the inhibitory activity of RRx-001, because the concentration required for NLRP3 inhibition was increased in the absence of the twin $NO_2$ groups. A possible explanation for this phenomenon is that the twin $NO_2$ groups may increase the binding affinity between RRx-001 and NLRP3 or may enhance the ability of RRx-001 to affect the NLRP3 conformation. We also found that RRx-001's bromoacetyl group is essential for the inhibitory activity of RRx-001 against NLRP3. Modification of the bromoacetyl group in RRx-001 abolished the inhibitory activity of RRx-001 and the interaction between RRx-001 and NLRP3. Since the inhibitory effect of RRx-001 is irreversible, we concluded that RRx-001 covalently binds to NLRP3 via its bromoacetyl group. As the C409A NACHT mutant could not interact with NLRP3, we confirmed that a covalent bond is formed between the bromoacetyl group and cysteine 409 in NLRP3. Further cocrystal structure studies need to be conducted to investigate how RRx-001 specifically binds with cysteine 409 and to evaluate the function of the twin $NO_2$ groups.

Moreover, DARTS assays with the cysteine mutants showed that the protective effect of RRx-001 was lower on the C319A and C463A NACHT mutants. It is possible that RRx-001 can interact with other cysteine residues of NLRP3 in addition to C409.

RRx-001 has been assessed in various phase I-II clinical trials for cancer treatment and is currently in a phase III clinical trial for the treatment of small cell lung cancer (SCLC).[28] Considering the enhanced and prolonged action of covalent drugs and the high safety of these drugs in clinical trials, our studies suggest that RRx-001 or its analogs might be effective and safe therapeutic agents for NLRP3-driven inflammatory diseases. However, as mentioned above, RRx-001 has many other targets, such as G6PD, and has an effect on the LPS-induced priming process. These functions may cause some side effects and might be a limitation to RRx-001's potential application as an NLRP3 inhibitor.

## MATERIALS AND METHODS

### Mice

C57BL/6J mice were purchased from the Shanghai SLAC Laboratory Animal Ltd. Corp. (Shanghai, China). *Nlrp3*$^{-/-}$ mice were described previously.[5] Mice were specific pathogen-free, maintained on a strict 12 h/12 h light/dark cycle (lights on at 8:00 a.m. and off at 8:00 p.m.). All animal experiment protocols were approved by the Animal Care Committee of the University of Science and Technology of China.

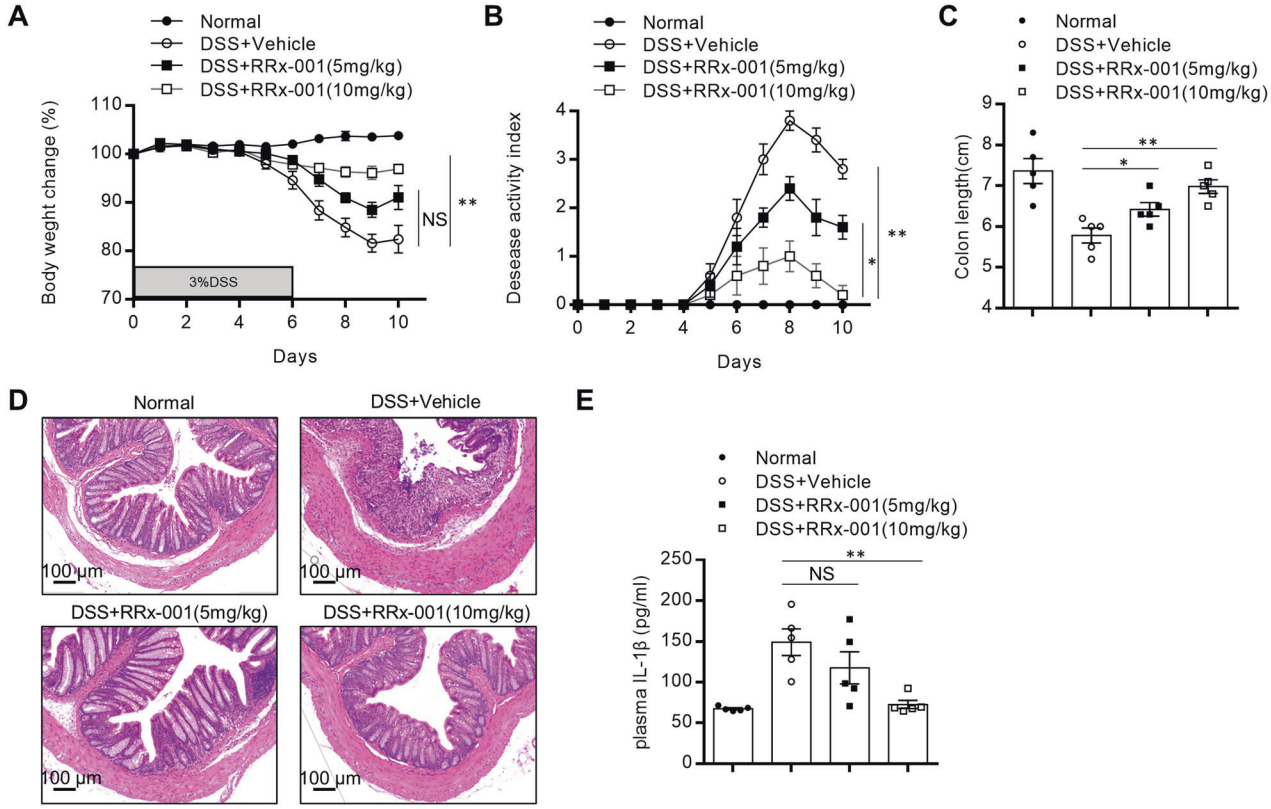


**Fig. 6 RRx-001 alleviates DSS-induced colitis in mice. A–E** Mice were treated with 3% DSS dissolved in the drinking water for 6 days and were then provided normal drinking water for 4 days. RRx-001 (5, 10 mg/kg) or vehicle were administered daily. Body weight loss (**A**), the disease activity index (DAI) (**B**), and colon length (**C**) were measured. **D** Sections of paraffin-embedded colon tissues were stained with H&E. **E** Plasma IL-1β levels were assessed by ELISA. The data are shown as the mean ± SEM values ($n = 5$) (**A**–**C**, **E**) or are representative of 5 mice (**D**). Statistical significance was analyzed by the Mann–Whitney test: $^{*}P < 0.05$; $^{**}P < 0.01$; NS not significant

Reagents

RRx-001 (S8405) was obtained from Selleck. Nigericin, ATP, MSU, DHEA and poly(A/T) were obtained from Sigma. Ultrapure LPS, Pam3CSK4, MitoTracker, MitoSOX, DAPI, MQAE, Lipofectamine 2000 and Lipofectamine RNAiMAX were obtained from Invitrogen. CL097 was obtained from InvivoGen. The *Salmonella* strain was a gift from Dr. Cai Zhang (Shandong University, Shandong, China). The TcdB toxin was a gift from Dr. Feng Shao (National Institute of Biological Sciences, Beijing, China). Anti-Flag antibody beads and protein G agarose were obtained from Sigma and Millipore, respectively. Anti-VSV (V4888) and anti-Flag (F2555) antibodies were obtained from Sigma. The anti-mouse IL-1β (p17) (AF-401-NA) antibody was obtained from R&D. Anti-mouse caspase-1 (p20) (AG-20B-0042) and anti-NLRP3 (AG-20B-0014) antibodies were obtained from Adipogen. The anti-NEK7 (ab133514) antibody was obtained from Abcam. The anti-ASC (67824) antibody was obtained from Cell Signaling Technology. The anti-β-actin (66009-1-Ig) antibody was obtained from Proteintech.

Cell preparation and stimulation

Bone marrow-derived macrophages and PBMCs were isolated and cultured as described.[19] To induce NLRP3 inflammasome activation, BMDMs ($5 \times 10^5$ cells/ml) or PBMCs ($1 \times 10^6$ cells/ml) were plated in 12-well plates, and the overnight culture medium was changed to Opti-MEM the following morning. Cells were primed with 50 ng/ml LPS or 400 ng/ml Pam3CSK4 (for noncanonical inflammasome activation) for 3 h and were then treated with RRx-001 for another 30 min. After that, cells were stimulated with MSU (150 μg/ml) or *S. typhimurium* (multiplicity of infection (MOI)) for 4 h, with ATP (2.5 mM) or nigericin (3 μM) for 30 min or with CL097 (30 μM) or TcdB toxin (0.5 μg/ml) for 1 h. Cells were also transfected with LPS (500 ng/ml) for 16 h or with poly(A/T) (0.5 μg/ml) for 4 h by using Lipofectamine 2000. Precipitated supernatants and cell extracts were analyzed by immunoblotting. LDH release was measured using an LDH Cytotoxicity Assay Kit (Beyotime).

SiRNA-mediated gene silencing in BMDMs

BMDMs ($3 \times 10^5$ cells/ml) were plated in 12-well plates. SiRNA (50 nM) was transfected into the cells in each well by using Lipofectamine RNAiMAX (Invitrogen) according to the manufacturer's instructions. The siRNA (si*G6pdx*) sequence was GAGGAGTTCTTTGCCCGTAAT.

Confocal microscopy

BMDMs ($2 \times 10^5$ cells/ml) were plated on coverslips (Thermo Fisher Scientific) in 12-well plates overnight. The next morning, BMDMs were stimulated with nigericin (3 μM) and stained with MitoTracker Red (50 nM) or MitoSOX (5 μM). Then, the supernatants were discarded, and the cells were washed with ice-cold PBS three times and fixed with 4% PFA in PBS for 15 min. After that, the cells were washed with PBST three times. Confocal microscopy analyses were carried out by using a Zeiss LSM 700.

Immunoblotting

Cell lysates were boiled in sample buffer at 100 °C for 10 min, and equal amounts of protein were loaded into the wells of an SDS-PAGE gel. The gel was run for 0.5 h at 80 V and for 1 h at 120 V. The transfer assembly was constructed with a PVDF membrane, and transfer was conducted at 90 V for 1 h. The membrane was blocked for 1 h at room temperature using blocking buffer (5%

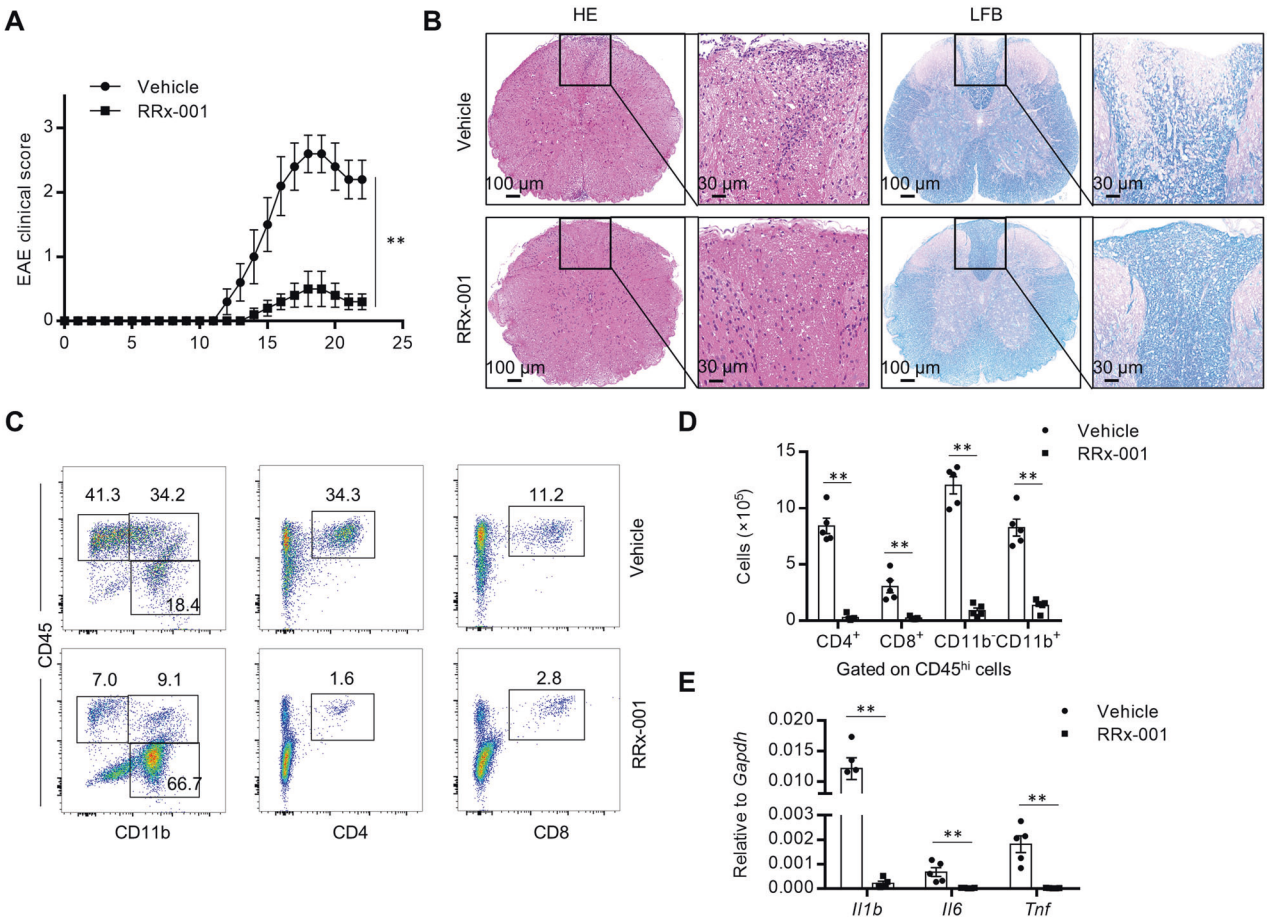


**Fig. 7 RRx-001 prevents the development of EAE. A–E** Mice were administered RRx-001 (10 mg/kg) or vehicle beginning at the induction of EAE every 2 days. **A** Clinical scores after EAE induction. **B** Sections of paraffin-embedded spinal cord tissues were stained with H&E or Luxol fast blue (LFB). Representative dot plots (**C**) and numbers (**D**) of live $CD4^+$, $CD8^+$, $CD11b^+$ and $CD11b^-$ cells gated on $CD45^{hi}$ cells from the mononuclear cell population in the CNS isolated on day 22 after EAE induction. **E** The expression levels of the indicated genes were assessed by real-time PCR. The data are shown as the mean ± SEM values ($n = 5$) (**A**, **D**, **E**) or are representative of 5 mice (**B**, **C**). Statistical significance was analyzed by the Mann–Whitney test: $^{**}P < 0.01$

nonfat milk) and was then incubated with the primary antibodies in blocking buffer overnight at 4 °C. The membrane was washed with PBST three times for 5 min each and was then incubated with the conjugated secondary antibodies in blocking buffer at room temperature for 1 h. The membrane was washed with PBST three times for 5 min each. Images were acquired after visualization by chemiluminescence.

ELISA

Cell culture and serum supernatants were assayed for mouse IL-1β, IL-6 or TNF-α and for human IL-1β or TNF-α according to the manufacturer's instructions (mouse IL-1β: R&D, DY-401; mouse TNF-α: R&D, DY410; mouse IL-6: R&D, DY406; human TNF-α: R&D, DY210; human IL-1β: BD, 557953).

Determination of intracellular potassium and chloride concentrations

To measure the intracellular potassium concentration, BMDMs plated in 6-well plates were stimulated to activate the NLRP3 inflammasome, and the culture medium was then discarded. Ultrapure $HNO_3$ was added to lyse cells, and the samples were boiled for 30 min at 100 °C. Then, $ddH_2O$ was added to dissolve the precipitated products. The potassium concentrations in the samples were measured by inductively coupled plasma optical emission spectrometry with a PerkinElmer Optima 7300 DV spectrometer.

To measure the intracellular chloride concentration, the culture medium of stimulated BMDMs in 12-well plates was discarded. Then, $ddH_2O$ was added and incubated for 15 min at 37 °C. The lysates were transferred to 1.5 ml EP tubes and centrifuged at 10,000 × *g* for 5 min. The supernatants were then mixed with 50 μl of MQAE (10 μM). The absorbance of the samples was measured in a BioTek Multi-Mode Microplate Reader (Synergy2). A control measurement of the extracellular amount of chloride was used for background subtraction in every experiment.

ASC oligomerization assay

After stimulation with nigericin (3 μM), BMDMs were rinsed in ice-cold PBS and were then lysed with NP-40 for 30 min at 4 °C. The lysates were centrifuged at 330 × *g* for 10 min at 4 °C. The pellets were washed three times with 1 ml of ice-cold PBS and resuspended in 500 μl of PBS. The resuspended pellets were incubated with 2 mM disuccinimidyl suberate (Sangon Biotech, C100015) for 30 min at room temperature. The samples were then centrifuged at 330 × *g* for 10 min at 4 °C. The crosslinked pellets were resuspended in 30 μl of sample buffer and were then analyzed by immunoblotting.

Immunoprecipitation

For the endogenous IP assay, BMDMs in 6-well plates were stimulated with nigericin (3 μM) and lysed with NP-40 lysis buffer containing complete protease inhibitor. Primary antibodies or IgG

(control) were added to the cell lysates, and Protein G Mag Sepharose was then added to the cell lysates. The cell lysates were incubated overnight at 4 °C with rotation. Antibody-bound proteins were precipitated by protein G beads and subjected to immunoblot analysis.

For the exogenous IP assay, HEK-293T cells in 6-well plates were transfected with plasmids by using polyethylenimine. After 24 h, cells were collected and lysed with NP-40 lysis buffer. Anti-Flag antibody–coated beads were used to immunoprecipitate the protein extracts. Then, the samples were analyzed by immunoblotting.

NLRP3 ATPase activity assay

Purified recombinant human proteins (1.4 ng/μl) were incubated with the indicated concentrations of RRx-001 at 37 °C for 15 min in reaction buffer. Then, ATP (25 μm, Ultra-Pure ATP) was added, and the mixture was incubated at 37 °C for another 40 min. The amount of ATP converted into adenosine diphosphate (ADP) was determined by luminescent ADP detection with an ADP-Glo Kinase Assay kit (Promega, Madison, MI, USA) according to the manufacturer's protocol. The results are expressed as the percentage of residual enzyme activity with respect to vehicle-treated enzyme activity.

Drug Affinity Responsive Target Stability (DARTS) assay

DARTS was carried out according to a published protocol.[53] BMDMs were primed with LPS (50 ng/ml) for 3 h. HEK-293T cells were harvested 24 h after transfection. Cells were lysed with NP-40 lysis buffer containing cOmplete protease inhibitor. Lysates were centrifuged at 12,000 × *g* for 10 min at 4 °C and the protein concentration was measured with a Pierce BCA Protein Assay Kit (Beyotime). Lysates were incubated with RRx-001 at the indicated concentrations overnight at 4 °C with rotation. Then, the protease pronase (25 ng of enzyme per μg of protein, Sigma) was added to the lysates (8 μg of protein lysate per reaction) and incubated for 30 min at room temperature. The reaction was stopped by the addition of 3×SDS loading buffer. Then, the samples were analyzed by immunoblotting.

Protein expression and purification

To produce the purified GFP-NLRP3 protein, the His-GFP-NLRP3 plasmid was transfected into HEK-293T cells. After 48 h, the cells were collected and lysed in lysis buffer (50 mM HEPES (pH 7.4), 150 mM NaCl, and 0.4% CHAPS) for 30 min. After sonication, the insoluble fraction was removed by centrifugation at 14,000 rpm for 15 min at 4 °C. The His-GFP-NLRP3 protein was initially purified by incubation with nickel–nitrilotriacetic acid matrices (QIAGEN) for 45 min at room temperature. Histidine precipitates were eluted in elution buffer after washing twice with lysis buffer. The eluted fractions were filtered through a 0.45 μm syringe filter and concentrated by an ultrafiltration device (Merck Millipore) to remove proteins <10 kD. Then, 5000 μl of the final eluted fractions was injected onto a Superdex 200 10/300 GL column (GE Healthcare). The protein was further purified in 50 mM HEPES (pH 7.4) and 150 mM NaCl on an AKTA purifier system (GE Healthcare). The fraction in each tube (10 μl each) was resolved by SDS-PAGE and detected by an anti-His antibody. The solutions in the tubes containing the His-GFP-NLRP3 protein were combined and concentrated with an ultrafiltration device (UFC910024; Merck Millipore) to remove proteins <100 kD.

Microscale thermophoresis assay

$K_D$ values were measured using a Monolith NT.115 instrument (NanoTemper Technologies). A range of concentrations of CY-09 (from 0.025 mM to 1.2 nM) were incubated with 200 nM purified His-GFP-NLRP3 protein for 40 min in assay buffer (50 mM HEPES, 10 mM MgCl2, 100 mM NaCl (pH 7.5), and 0.05% Tween 20). The samples were loaded into NanoTemper glass capillaries, and MST was performed using an LED power of 100% and an MST power of 80%. $K_D$ values were calculated using the mass action equation with NanoTemper software from duplicate reads of an experiment.

Plasmid construction

PCR was performed using PrimeSTAR® Max DNA Polymerase (TaKaRa). Restriction enzymes were purchased from Thermo Fisher Scientific. Gene recombination was performed using a ClonExpress® II One Step Cloning Kit (Vazyme). All fragments amplified by PCR were sequenced in the final plasmids. To generate NACHT mutants, primers were used to generate pCR3-Flag-NLRP3 linear DNA, and recombinant plasmids were constructed using the ClonExpress® II One Step Cloning Kit (Vazyme). To generate pLEX-NLRP3(C405A), primers were used to generate pLEX-NLRP3 linear DNA. Recombinant plasmids were constructed using the ClonExpress® II One Step Cloning Kit (Vazyme).

NLRP3 reconstitution

*Nlrp3*$^{-/-}$ BMDMs were plated in 12-well plates overnight and were then transduced with cDNA encoding mouse NLRP3 or NLRP3 (C409A) using the pLEX lentiviral expression vector (Thermo Fisher). After 6 h, the culture medium was replaced with DMEM supplemented with 10% FBS. After 2 days, BMDMs were stimulated in accordance with a standard protocol.

Assessment of LPS-induced systemic inflammation

Eight-week-old male C57BL/6 mice (body weight: control group, 24.46 ± 0.411 g; LPS + vehicle group, 24.56 ± 0.248 g; LPS + RRx-001 group, 24.6 ± 0.397 g) were intraperitoneally injected with RRx-001 (10 mg/kg) or vehicle containing 90% PBS and 10% DMSO and then intraperitoneally injected with LPS (20 mg/kg). After 4 h, serum samples were collected, and cytokines were measured by ELISA.

Induction and assessment of DSS-induced Colitis

Eight-week-old male C57BL/6 mice (body weight: control group, 23.54 ± 0.204 g; DSS + vehicle group, 25.06 ± 0.37 g; DSS + RRx-001 (5 mg/kg) group, 24.84 ± 0.304 g; DSS + RRx-001 (10 mg/kg) group: 24.86 ± 0.564 g) were treated with 3% DSS (MP Biomedicals) dissolved in the drinking water for 6 days and were then provided normal drinking water for 4 days. Control group mice were given regular water. RRx-001 was intraperitoneally injected into mice (5 or 10 mg/kg) beginning at disease induction every day for 10 days. Control group mice were injected with vehicle containing 90% PBS and 10% DMSO at the same time points. Body weight was measured every day. The disease activity index (DAI) was scored on a scale of 0–4 as follows: 0, normal stools; 1, soft stools; 2, soft stools and slight bleeding; 3, loose stools and slight bleeding; and 4, gross bleeding. Mice were sacrificed on day 10 to measure colon length.

Induction and assessment of EAE

Eight-week-old male C57BL/6 mice (body weight: vehicle group, 24.74 ± 0.248 g; RRx-001 group, 24.96 ± 0.331 g) or *Nlrp3*$^{-/-}$ mice (body weight: vehicle group, 24.52 ± 0.25 g; RRx-001 group, 24.6 ± 0.315 g) were injected subcutaneously in the dorsal flanks with 3 mg/ml $MOG_{35-55}$ peptide (300 μg per mouse) in CFA containing 5 mg/ml heat-killed *Mycobacterium tuberculosis* (500 μg per mouse) on day 0. Pertussis toxin (150 ng per mouse, list labs) was given i.v. on days 0 and 2. RRx-001 was intraperitoneally injected into mice (10 mg/kg) beginning at disease induction every 2 days for 22 days. Control group mice were injected with vehicle containing 90% PBS and 10% DMSO at the same time points. Disease severity was scored on a scale of 0–5 as follows: 0, no abnormalities; 1, limp tail or waddling gait with tail tonicity; 2, wobbly gait; 3, hind limb paralysis; 4, hind limb and forelimb paralysis; 5, death. To analyze CNS infiltrates, both the brain and spinal cord were harvested from mice perfused with PBS, and mononuclear cells were isolated by 30% Percoll separation.

Histological analysis

Mouse colons and spinal cords were postfixed with 4% PFA for 24 h and sectioned after embedding in paraffin. Sections were prepared and stained with H&E or LFB using standard procedures. Slides were examined under a Nikon ECL IPSE Ci biological microscope, and images were acquired with a Nikon DS-U3 color digital camera.

Quantitative real-time PCR

Total RNA was isolated from BMDMs or tissues by extraction with TRIzol reagent (Takara). RNA (800 ng) from each sample was used for reverse transcription with Moloney murine leukemia virus (M-MLV) reverse transcriptase (Invitrogen) according to the manufacturer's instructions. Quantitative PCR was performed using SYBR Green premix (Takara Bio) in a Roche LightCycler 96. *Gapdh* was used as the reference gene. The sequences of the gene-specific primers used were as follows:

mouse *G6pdx* forward, GCACTTTGTCCGGAGTGATG;
mouse *G6pdx* reverse, AAGGGAAGATGCAGAAAGGGT;
mouse *Il1b* forward, TGCCACCTTTTGACAGTGATG;
mouse *Il1b* reverse, AAGGTCCACGGGAAAGACAC;
mouse *Il6* forward, GTCCTTCCTACCCCAATTTCC;
mouse *Il6* reverse, GCACTAGGTTTGCCGAGTAGA;
mouse *Tnf* forward, CGATGGGTTGTACCTTGTC;
mouse *Tnf* reverse, CGGACTCCGCAAAGTCTAAG;
mouse *Gapdh* forward, GGTGAAGGTCGGTGTGAACG;
mouse *Gapdh* reverse, CTCGCTCCTGGAAGATGGTG.

Statistical analyses

All values are expressed as the means ± SEMs. Statistical analysis was carried out using the Mann–Whitney test (GraphPad Software) for all data with a normal distribution. No data points were excluded. The researchers were not blinded to the allocation of treatment groups during sample collection and data analysis. Sample sizes were selected on the basis of preliminary results to ensure adequate power. Differences between data were considered significant when the $P$ value was $<0.05$.

## ACKNOWLEDGEMENTS

We thank Dr. Feng Shao (National Institute of Biological Sciences, Beijing, China) for providing the TcdB toxin. This research was supported by the National Key Research and Development Program of China (grant numbers 2019YFA0508503 and 2020YFA0509101), the Strategic Priority Research Program of the Chinese Academy of Sciences (grant number XDB29030102), the National Natural Science Foundation of China (grant numbers 82003765, 81821001, 31770991, and 91742202), the Fundamental Research Funds for the Central Universities and the University Synergy Innovation Program of Anhui Province (GXXT-2019-026), the Natural Science Foundation of Anhui Province (1908085QC99) .

## AUTHOR CONTRIBUTIONS

Y.C., H.H. and B.L performed the experiments of this work; X.D., W.J. and R.Z. designed the research. Y.C., W.J. and R.Z. wrote the manuscript. W.J. and R.Z. supervised the project.

## ADDITIONAL INFORMATION

**Supplementary information** The online version contains supplementary material available at https://doi.org/10.1038/s41423-021-00683-y.

**Competing interests:** R.Z., W.J. and Y.C. are named as inventors on China National Intellectual Property Administration Application Serial No. 202011472140.0 related to RRx-001.

## REFERENCES

1. Martinon, F., Mayor, A. & Tschopp, J. The Inflammasomes: guardians of the Body. *Annu. Rev. Immunol.* **27**, 229–265 (2009).
2. Davis, B. K., Wen, H. T. & Ting, J. P. Y. The inflammasome NLRs in immunity, inflammation, and associated diseases. *Annu. Rev. Immunol.* **29 29**, 707–735 (2011).
3. Chen, G., Shaw, M. H., Kim, Y. G. & Nunez, G. NOD-like receptors: role in innate immunity and inflammatory disease. *Annu Rev. Pathol.-Mech.* **4**, 365–398 (2009).
4. Broz, P. & Dixit, V. M. Inflammasomes: mechanism of assembly, regulation and signalling. *Nat. Rev. Immunol.* **16**, 407–420 (2016).
5. Martinon, F., Petrilli, V., Mayor, A., Tardivel, A. & Tschopp, J. Gout-associated uric acid crystals activate the NALP3 inflammasome. *Nature* **440**, 237–241 (2006).
6. Masters, S. L. et al. Activation of the NLRP3 inflammasome by islet amyloid polypeptide provides a mechanism for enhanced IL-1beta in type 2 diabetes. *Nat. Immunol.* **11**, 897–904 (2010).
7. Wen, H. et al. Fatty acid-induced NLRP3-ASC inflammasome activation interferes with insulin signaling. *Nat. Immunol.* **12**, 408–415 (2011).
8. Unamuno, X. et al. NLRP3 inflammasome blockade reduces adipose tissue inflammation and extracellular matrix remodeling. *Cell Mol. Immunol.* **18**, 1045–1057 (2021).
9. He, Y. et al. Immunopathobiology and therapeutic targets related to cytokines in liver diseases. *Cell Mol. Immunol.* **18**, 18–37 (2021).
10. Heneka, M. T. et al. NLRP3 is activated in Alzheimer's disease and contributes to pathology in APP/PS1 mice. *Nature* **493**, 674–678 (2013).
11. Duewell, P. et al. NLRP3 inflammasomes are required for atherogenesis and activated by cholesterol crystals. *Nature* **464**, 1357–1361 (2010).
12. Bauer, C. et al. Colitis induced in mice with dextran sulfate sodium (DSS) is mediated by the NLRP3 inflammasome. *Gut* **59**, 1192–1199 (2010).
13. Zaki, M. H. et al. The NLRP3 inflammasome protects against loss of epithelial integrity and mortality during experimental colitis. *Immunity* **32**, 379–391 (2010).
14. Lamkanfi, M. & Dixit, V. M. Inflammasomes and their roles in health and disease. *Annu Rev. Cell Dev. Biol.* **28**, 137–161 (2012).
15. He, Y. et al. 3,4-Methylenedioxy-beta-nitrostyrene Inhibits NLRP3 Inflammasome Activation by Blocking Assembly of the Inflammasome. *J. Biol. Chem.* **289**, 1142–1150 (2014).
16. Coll, R. C. et al. A small-molecule inhibitor of the NLRP3 inflammasome for the treatment of inflammatory diseases. *Nat. Med.* **21**, 248–255 (2015).
17. Jiang, H. et al. Identification of a selective and direct NLRP3 inhibitor to treat inflammatory disorders. *J. Exp. Med.* **214**, 3219–3238 (2017).
18. Huang, Y. et al. Tranilast directly targets NLRP3 to treat inflammasome-driven diseases. *EMBO Mol. Med.* **10**, e8689 (2018).
19. He, H. et al. Oridonin is a covalent NLRP3 inhibitor with strong anti-inflammasome activity. *Nat. Commun.* **9**, 2550 (2018).
20. Marchetti, C. et al. OLT1177, a beta-sulfonyl nitrile compound, safe in humans, inhibits the NLRP3 inflammasome and reverses the metabolic cost of inflammation. *Proc. Natl Acad. Sci. USA* **115**, E1530–E1539 (2018).
21. Coll, R. C. et al. MCC950 directly targets the NLRP3 ATP-hydrolysis motif for inflammasome inhibition. *Nat. Chem. Biol.* **15**, 556–559 (2019).
22. Mullard, A. NLRP3 inhibitors stoke anti-inflammatory ambitions. *Nat. Rev. Drug Disco.* **18**, 405–407 (2019).
23. Kluck, V. et al. Dapansutrile, an oral selective NLRP3 inflammasome inhibitor, for treatment of gout flares: an open-label, dose-adaptive, proof-of-concept, phase 2a trial. *Lancet Rheumatol.* **2**, e270–e280 (2020).
24. Oronsky, B. et al. Rockets, radiosensitizers, and RRx-001: an origin story part I. *Disco. Med* **21**, 173–180 (2016).
25. Kim, M. M. et al. Whole brain radiotherapy and RRx-001: two partial responses in radioresistant melanoma brain metastases from a phase I/II clinical trial: a TITE-CRM phase I/II clinical trial. *Transl. Oncol.* **9**, 108–113 (2016).
26. Carter, C. et al. Early results: "Rocket" a Phase II Study of Rrx-001, a novel triple epigenetic inhibitor, resensitization to irinotecan in colorectal cancer. *Ann. Oncol.* **26**, ii3 (2015).
27. Morgensztern, D. et al. RRx-001 followed by platinum plus etoposide in patients with previously treated small-cell lung cancer. *Br. J. Cancer* **121**, 211–217 (2019).
28. Oronsky, B. et al. REPLATINUM Phase III randomized study: RRx-001 + platinum doublet versus platinum doublet in third-line small cell lung cancer. *Future Oncol.* **15**, 3427–3433 (2019).
29. Carter, C. A. et al. Partial response to platinum doublets in refractory EGFR-positive non-small cell lung cancer patients after RRx-001: evidence of epi-sensitization. *Case Rep. Oncol.* **9**, 62–67 (2016).
30. Oronsky, B. et al. RRx-001: a systemically non-toxic M2-to-M1 macrophage stimulating and prosensitizing agent in Phase II clinical trials. *Expert Opin. Investig. Drugs* **26**, 109–119 (2017).
31. Oronsky, B. et al. RRx-001, a novel dinitroazetidine radiosensitizer. *Invest N. Drugs* **34**, 371–377 (2016).
32. Scicinski, J. et al. Preclinical evaluation of the metabolism and disposition of RRx-001, a novel investigative anticancer agent. *Drug Metab. Dispos.* **40**, 1810–1816 (2012).

33. Zhao, H. et al. Epigenetic effects of RRx-001: a possible unifying mechanism of anticancer activity. *Oncotarget* **6**, 43172–43181 (2015).
34. Oronsky, B., Scicinski, J., Cabrales, P. & Minchinton, A. RRx-001, an epigenetic-based radio- and chemosensitizer, has vascular normalizing effects on SCCVII and U87 tumors. *Clin. Epigenetics* **8**, 53 (2016).
35. Cabrales, P. RRx-001 acts as a dual small molecule checkpoint inhibitor by downregulating CD47 on cancer cells and SIRP-alpha on monocytes/macrophages. *Transl. Oncol.* **12**, 626–632 (2019).
36. Oronsky, B., Scribner, C., Aggarwal, R. & Cabrales, P. RRx-001 protects normal tissues but not tumors via Nrf2 induction and Bcl-2 inhibition. *J. Cancer Res Clin. Oncol.* **145**, 2045–2050 (2019).
37. Reid, T. et al. Safety and activity of RRx-001 in patients with advanced cancer: a first-in-human, open-label, dose-escalation phase 1 study. *Lancet Oncol.* **16**, 1133–1142 (2015).
38. Gross, C. J. et al. K+ efflux-independent NLRP3 inflammasome activation by small molecules targeting mitochondria. *Immunity* **45**, 761–773 (2016).
39. Yu, W. et al. One-carbon metabolism supports S-adenosylmethionine and histone methylation to drive inflammatory macrophages. *Mol. Cell* **75**, 1147–1160 e1145 (2019).
40. Oronsky, B. et al. RRx-001, a novel clinical-stage chemosensitizer, radiosensitizer, and immunosensitizer, inhibits glucose 6-phosphate dehydrogenase in human tumor cells. *Disco. Med* **21**, 251–265 (2016).
41. Petrilli, V. et al. Activation of the NALP3 inflammasome is triggered by low intracellular potassium concentration. *Cell Death Differ.* **14**, 1583–1589 (2007).
42. Munoz-Planillo, R. et al. K(+) efflux is the common trigger of NLRP3 inflammasome activation by bacterial toxins and particulate matter. *Immunity* **38**, 1142–1153 (2013).
43. Daniels, M. J. et al. Fenamate NSAIDs inhibit the NLRP3 inflammasome and protect against Alzheimer's disease in rodent models. *Nat. Commun.* **7**, 12504 (2016).
44. Tang, T. et al. CLICs-dependent chloride efflux is an essential and proximal upstream event for NLRP3 inflammasome activation. *Nat. Commun.* **8**, 202 (2017).
45. Zhou, R., Yazdi, A. S., Menu, P. & Tschopp, J. A role for mitochondria in NLRP3 inflammasome activation. *Nature* **469**, 221–225 (2011).
46. Xie, J. H., Li, Y. Y. & Jin, J. The essential functions of mitochondrial dynamics in immune cells. *Cell Mol. Immunol.* **17**, 712–721 (2020).
47. Lu, A. et al. Unified polymerization mechanism for the assembly of ASC-dependent inflammasomes. *Cell* **156**, 1193–1206 (2014).
48. Dick, M. S., Sborgi, L., Ruhl, S., Hiller, S. & Broz, P. ASC filament formation serves as a signal amplification mechanism for inflammasomes. *Nat. Commun.* **7**, 11929 (2016).
49. He, Y., Zeng, M. Y., Yang, D., Motro, B. & Nunez, G. NEK7 is an essential mediator of NLRP3 activation downstream of potassium efflux. *Nature* **530**, 354–357 (2016).
50. Shi, H. X. et al. NLRP3 activation and mitosis are mutually exclusive events coordinated by NEK7, a new inflammasome component. *Nat. Immunol.* **17**, 250–258 (2016).
51. Schmid-Burgk, J. L. et al. A genome-wide CRISPR (clustered regularly interspaced short palindromic repeats) screen identifies NEK7 as an essential component of NLRP3 inflammasome activation. *J. Biol. Chem.* **291**, 103–109 (2016).
52. Haq, T. et al. Mechanistic basis of Nek7 activation through Nek9 binding and induced dimerization. *Nat. Commun.* **6**, 8771 (2015).
53. Lomenick, B. et al. Target identification using drug affinity responsive target stability (DARTS). *Proc. Natl Acad. Sci. USA* **106**, 21984–21989 (2009).
54. Scicinski, J. et al. NO to cancer: the complex and multifaceted role of nitric oxide and the epigenetic nitric oxide donor, RRx-001. *Redox Biol.* **6**, 1–8 (2015).
55. He, Y., Franchi, L. & Nunez, G. TLR agonists stimulate Nlrp3-dependent IL-1beta production independently of the purinergic P2X7 receptor in dendritic cells and in vivo. *J. Immunol.* **190**, 334–339 (2013).
56. Gris, D. et al. NLRP3 plays a critical role in the development of experimental autoimmune encephalomyelitis by mediating Th1 and Th17 responses. *J. Immunol.* **185**, 974–981 (2010).
57. Inoue, M., Williams, K. L., Gunn, M. D. & Shinohara, M. L. NLRP3 inflammasome induces chemotactic immune cell migration to the CNS in experimental autoimmune encephalomyelitis. *Proc. Natl Acad. Sci. USA* **109**, 10480–10485 (2012).
58. Sharif, H. et al. Structural mechanism for NEK7-licensed activation of NLRP3 inflammasome. *Nature* **570**, 338–343 (2019).